Research Article

Research on the Seismic Performance of Prefabricated Bridge Piers Using UHPC Grout under an Eccentric Load

Ben Zeng [1], **Jiahui Xu,** [1] **Xiaohong Zheng** [2], **and Songqi Zhang** [3]

[1]*Guangzhou Urban Planning and Design Survey Research Institute, Guangzhou 510060, China*
[2]*School of Civil Engineering and Transportation, South China University of Technology, Guangzhou 510640, China*
[3]*Guangzhou Metro Construction Management Co., Ltd., Guangzhou 511430, China*

Correspondence should be addressed to Xiaohong Zheng; xhzheng@scut.edu.cn

At present, research on prefabricated piers is limited to the axial compression state. However, many piers are under small eccentric compression in practical engineering. In this article, the seismic performance of ultrahigh performance concrete (UHPC)-grouted corrugated pipe-connected piers under small eccentric compression was studied. A pseudostatic test was carried out by using a prefabricated pier column model connected with UHPC-grouted corrugated pipes. The failure mechanism of the plastic hinge area of the column base was studied, and the failure mode, energy dissipation capacity, displacement ductility, and ultimate bearing capacity were compared with those of an ordinary axially compressed pier column structure. The result shows that compared to the conventional cast-in-place(CIP) pier, the overall energy dissipation capacity and the ductility factor of assembled pier with UHPC-grouted corrugated pipe-connection were decreased approximately by 5.0% and by 10%, respectively. The pinching phenomenon of the hysteresis curve of the precast pier was more obvious. When the assembled piers were under small eccentric compression, the overall energy dissipation capacity was close to that of conventional CIP piers and the ductility factor was improved by 20%. Comparison of two precast piers using the same UHPC grout connections shows that the stiffness degradation process of precast pier under small eccentric compression was similar to that under axial compression. But the ductility coefficient of precast pier under small eccentric compression increased by about 20%. The small eccentric compression caused different damage degrees in the plastic hinge zone at the bottom of the precast column. The ultimate load in the same direction as the additional bending moment was 55% lower than that of the opposite direction.

1. Introduction

Prefabricated assembly technology was first applied to the superstructure of bridges, and now it is mature in terms of design and construction. The prefabricated assembly methodology of bridge substructures is slowly developing and has been gradually applied in practical engineering in recent years [1, 2]. At present, the connection methods of precast and assembled piers mainly include posttensioned prestressed reinforcement connections, wet joint connections, socket connections, grouting sleeve connections, corrugated pipe connections, and shape memory alloy (SMA) washer spring-basedself-centering rocking (SCR) systems [3–8]. As for the prefabricated bridge piers, the

columns and the rest of the structures are precast independently and then assembled into a whole by using different connections. The connection position is weak because the reinforced bars of each element are disconnected. In seismic regions, the seismic performance of connecting joint is the primary concern because the columns must dissipate the earthquake energy while maintaining the structural integrity. The connections with corrugated pipes shown in Figure 1 that represent a widely used prefabricated assembly technology for connecting cover beams with pier columns and connecting pier columns with pier caps because they require less on-site construction work and offer fast assembly, low processing accuracy, and reliable connectivity [9–11]. In 2018, Jia et al. [12] performed a seismic

test on prefabricated piers and columns connected with corrugated pipes in areas with a high seismic activity, showing that corrugated pipe connections are reliable, exhibit favorable performance, and can be applied as connections between piers and pier caps in areas with strong seismic activity.

Ultrahigh performance concrete (UHPC) is a cement-based composite material with ultrahigh strength, ductility, and durability. The application of UHPC in many bridge projects has proven that using this material is a feasible way to solve many technical problems in current bridge structures. Due to the high bonding strength between UHPC and steel bars [13], their coordinated deformation and workability are much better than those of ordinary steel-concrete structures [14, 15]. Therefore, applying UHPC to the connections of prefabricated bridges can significantly improve their seismic performance. In 2015, Chen et al. [16] performed a pull-out test examining the bond and anchorage performance between steel bars and the high-strength grouting material in pre-embedded corrugated pipes, and Qiu et al. [17] studied the seismic performance of piers prefabricated with prestressed corrugated pipes, showing that the connection performance of corrugated pipes is reliable and that their construction is simple. Tazarv and Saiidi [18] performed quasistatic experimental research on two prefabricated pier models, showing that the seismic performance of UHPC-grouted corrugated pipe connections is better than that of traditional cast-in-place connections.

At present, experimental research on the connection structures and seismic performance of prefabricated piers is limited to the axial compression state [19–22], and there is rarely relevant research or analysis on the seismic performance of prefabricated piers under eccentric loads available in the literature. Actually, most of the prefabricated bridge piers are under small eccentric compression, which is very limited in existing studies. In order to simulate the stress situation closer to the actual assembled bridge pier, small eccentricity loading and prefabricated connection were considered in this study. In this article, three model specimens were designed according to the actual viaduct engineering in Guangzhou city, and the scale ratio was 1 : 2.35. A series of pseudostatic tests considering eccentric compression were carried out to study the seismic performance of the prefabricated bridge piers connected by the UHPC-grouted corrugated pipe. The objective of this research is verify the validity and reliability of prefabricated bridge piers connected by UHPC grout under eccentric compression. It is of great scientific significance to provide data basis for the application of UHPC grout connection technology in the practical projects.

2. Materials and Methods

2.1. Design of Model and Specimens. A viaduct under construction is used as an example, as shown in Figure 2. The viaduct is a twin-deck bridge with a total deck width of 25 m. The superstructure of the bridge is a prefabricated small box girder, and the substructure is a double-column rectangular

cap beam-pier system. Due to the unequal adjacent spans, some piers are under eccentric compression. When the 35 m span is fully loaded and the 25 m span is unloaded, this part of the bridge pier column is under the worst load distribution; at this time, the unbalanced bending moment is 553.5 kN·m, the braking force is 320 kN, and the axial pressure is 2353 kN. According to calculation and analysis, the reinforcement ratio under this pier column section is 1.51%, and the eccentricity of the actual cover beam is 0.235 m.

This test is based on the principle of similarity of the actual reinforcement ratio calculated as the basis for subsequent research, and some similarity constants of the model are obtained from the similarity criterion after the basic parameters, such as the reinforcement ratio, are determined. According to the limitations of laboratory loading conditions and space, the scaling ratio in this test was designed to be 1 : 2.35, so the converted eccentricity is 0.1 m.

2.2. Determination of a Multifactor Test Model. This study mainly focuses on the seismic performance of fabricated bridge piers under eccentric loads, involving two independent variables, namely, the component connection type and the loading position, and each of the independent variables contains two levels. According to the multifactor experimental design method, this test requires $2 \times 2 = 4$ sets of specimens to determine the impact of each variable on the seismic performance of the bridge piers. Since the combination of the cast-in-place structure level and the independent variable (the loading position) level has no obvious effect on the seismic performance of the bridge pier, the combination of the cast-in-place structure level and the independent variable level of the loading position is ignored; the final experimental models are shown in Figure 3 and Table 1.

2.3. Material Properties

2.3.1. Concrete. The concrete is self-compacting commercial concrete with a strength grade of C40. A concrete test block is reserved when grouting the specimens. The measured elastic modulus of the concrete is 34000 MPa, and the compressive strength is 51.19 MPa.

2.3.2. Reinforcing Bars. The steel bars used in the specimen is HRB400 hot-rolled ribbed steel, the diameters of the longitudinal bar of the specimen and the main bar in the cap are 25 mm, and the diameter of the tie bar is 16 mm. The measured performance of the main reinforcement is shown in Table 2.

2.3.3. UHPC Grouting Material. The grouting material in the corrugated pipes is UHPC. The compressive strength test of the UHPC is determined with a 100 mm × 100 mm cube specimen, and the 28-day compressive strength of the measured UHPC is 116.03 MPa.

(a)

(b)

FIGURE 1: Prefabricated piers and columns connected with corrugated pipes [2]. (a) Prefabricated piers. (b) Corrugated pipes.
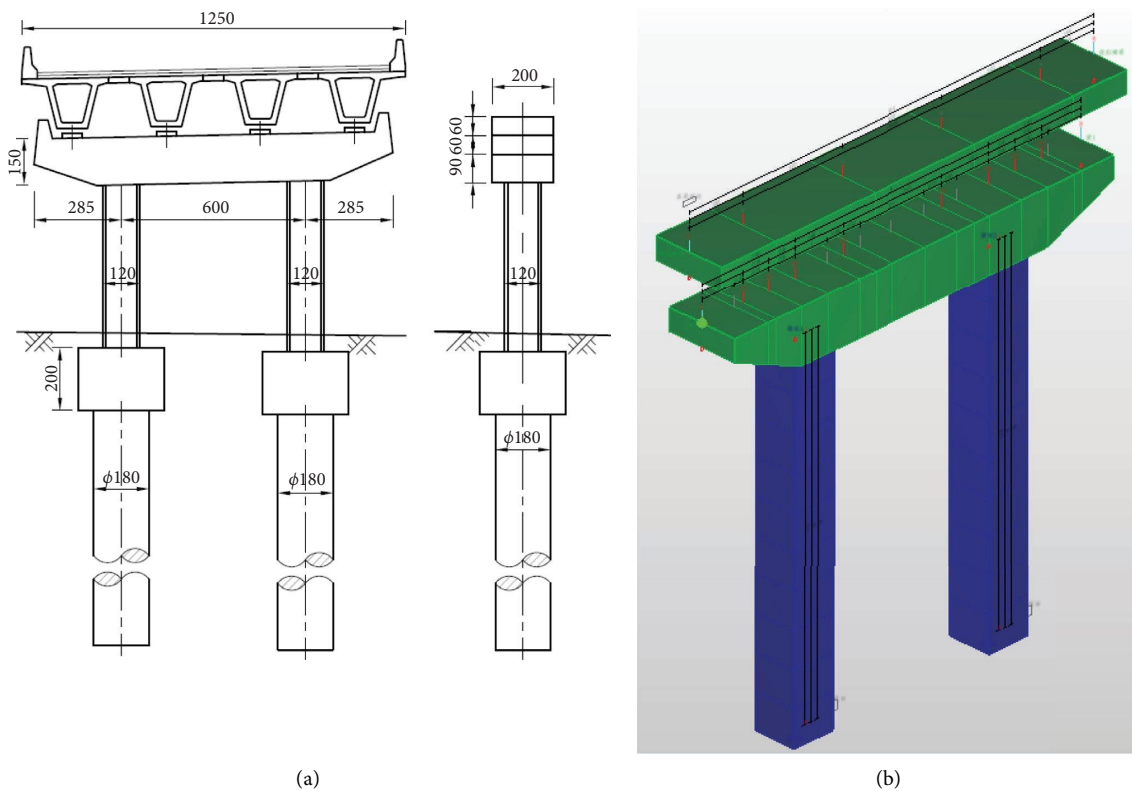

(a)

(b)

FIGURE 2: Overview of the prototype and finite element model. (a) The cross-section view (unit: cm). (b) The finite element model.

2.4. Test Equipment and the Measurement System. The test is performed with a large-scale mechanical testing and simulation (MTS, a company from the United States) electro-hydraulic servo loading system, and a schematic diagram of the loading device and the actual loading situation are shown in Figure 4.

The axial compression ratio of the test is taken as $\eta_k = 0.1$. In this test, loading is applied by the mixed control of force and displacement. In the loading test, the incremental load of each level is set to 40 kN, and each level of load is cycled once until the specimen yields. After the specimen reaches the yield displacement, it is loaded according to an integer multiple of the yield displacement, and each load level is cycled 3 times until the specimen is obviously damaged or

the horizontal bearing capacity of the specimen is reduced to 85% of the ultimate horizontal load.

3. Results

3.1. Distribution of Cracks in Piers. The distribution of cracks on the loading surface of the pier column of each specimen was shown in Figure 5(a). Compared with the CIP specimen A1, the crack distribution of prefabricated specimens (B1 and B2) connected by UHPC-grouted corrugated pipes indicated similar pattern. The crack spreading height of B1 is the highest among three specimens. The space between cracks near the bottom of the pier column of B1 is denser, while larger at the upper location than that of specimens A1

TABLE 1: Grouping of the experimental model.

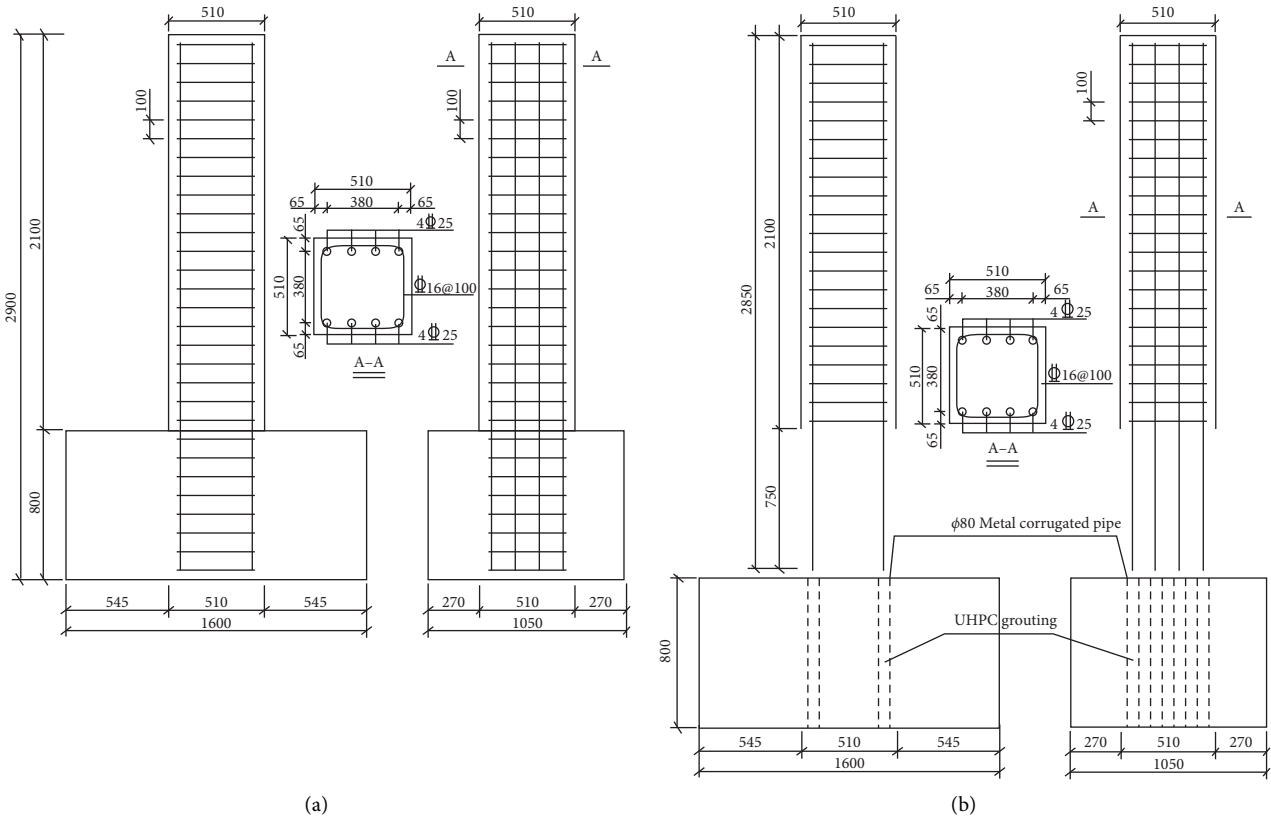| Groups	Types	Longitudinal reinforcing bar diameter (mm)	Single pier area (mm^2)	Number of Piers	Sectional area (mm^2)	Reinforcement ratio (%)
A	Cast-in-place + axial load	25	490.9	8	510×510	1.51
B1	UHPC-grouted corrugated pipe + axial load	25	490.9	8	510×510	1.51
B2	UHPC-grouted corrugated pipe + eccentric load	25	490.9	8	510×510	1.51

Figure 3: Schematic diagram of specimen reinforcement. (a) Specimen A and (b) specimen B1/B2.

Table 2: Measured material properties of steel.

Diameter (mm)	Yield load (kN)	Ultimate load (kN)	Yield strength (MPa)	Ultimate strength (MPa)	Elastic modulus (GPa)
25	218.51	301.93	445.12	615.05	205.46

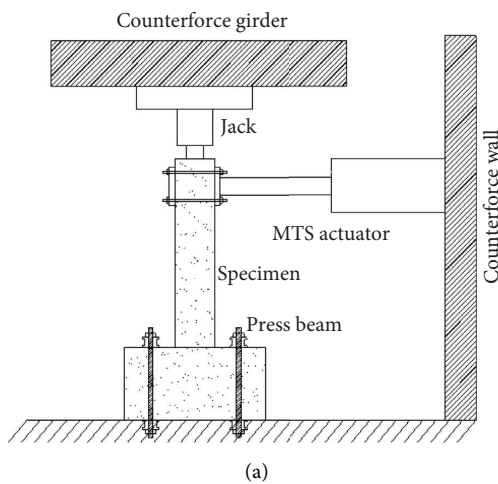Figure 4: Loading device. (a) Schematic diagram of the loading device. (b) Photograph of the loading device.

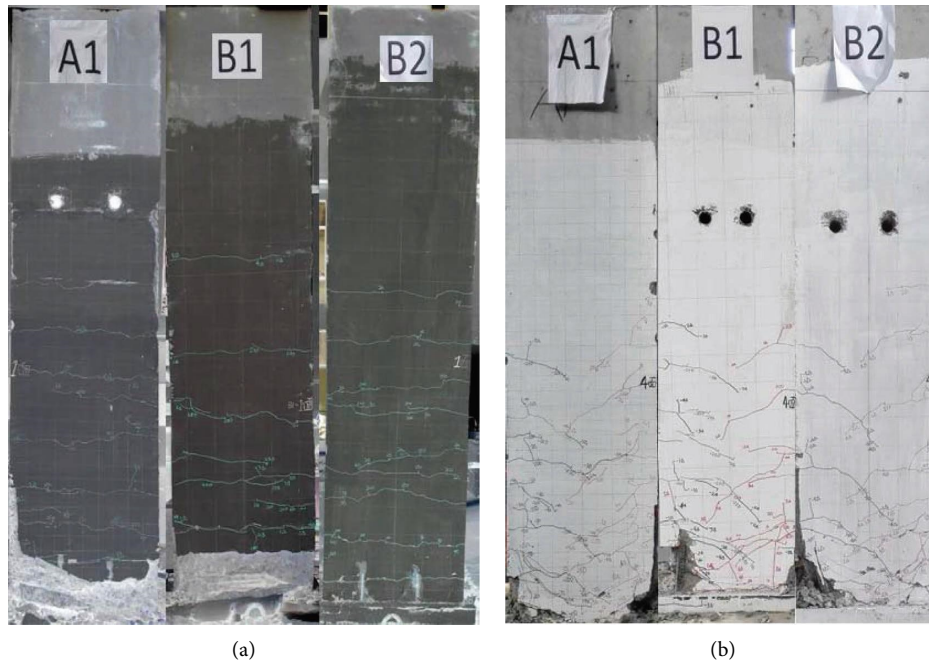(a)   (b)

FIGURE 5: Distribution of cracks in pier columns. (a) Loading surface. (b) Side surface.

and B2. Mainly because the longitudinal reinforcement bars at the foot of the pier column were strongly bonded by UHPC grout. The crack distribution of B1 and B2 specimens is similar from Figure 5(a). The difference was that the concrete at the bottom of the B1 pier column was more seriously damaged. In general, a small bias load has a little effect on the crack distribution on the loading surface.

The comparison of the crack distribution on the side surface is shown in Figure 5(b). It can be seen that the cracks pattern of A1 and B1 under axial compression is similar, which are basically symmetrical, developing down in an oblique direction. Specimen B1 has higher side crack, which indicated that the force can be transferred effectively by using the UHPC-grouted corrugated pipe connection. The influence of eccentricity on side cracks is obvious for specimen B2 from Figure 5(b). The cracks extended to different lengths towards two sides. There were more and longer cracks on the tensile side than that on the eccentric compression side. In addition, concrete at the column foot on the eccentric side was crushed more seriously.

3.2. Plastic Hinge Area. The distribution of cracks in the plastic hinge area for each specimen is shown in Figure 6 indicating similar pattern generally. Compared with the CIP specimen A1, the cracks in the plastic hinge area of specimen B1 connected with the UHPC-grouted corrugated pipe were denser, but the concrete crush depth was slightly shallower than that of specimen A1. As for specimen B2, which was under a small eccentric load, the cracks extended longer from the eccentric side to the opposite side, and the concrete at the column foot on the eccentric side was more seriously crushed. The reason was that the eccentric pressure caused an additional bending moment which increased the

compressive stress at the eccentric side. Therefore, the effect of small eccentric load was to cause different failure degrees on two sides at the bottom of the column foot.

4. Discussion

4.1. Hysteresis Curve. As shown in Figure 7, in the early stage of loading, each specimen is basically in the elastic stage, and the hysteresis loops are more overlapped and concentrated. The hysteresis loop of the specimen gradually opens with the increasing load-displacement level and number of cycles. The yield displacement of specimen B1 is slightly different from that of the specimens in Group A. The hysteresis loops are basically coincident, and the UHPC-grouted corrugated pipe arrangement in specimen B1 can achieve the same effect as the cast-in-place specimen and shows a stronger energy dissipation capacity.

In specimen B2, under eccentric compression, the center symmetry characteristic of the hysteresis curve is weakened. Eccentric axial compression is equivalent to axial compression plus an additional bending moment on the pier. During positive loading, the additional bending moment and the horizontal load act synergistically; during negative loading, the additional bending moment and the horizontal load counteract each other. Thus, in the positive displacement of the hysteresis curve in the force control stage, the positive displacement generated at the same force load level is greater than the negative displacement; in the displacement control stage, the positive bearing capacity generated at the same displacement load level is smaller than the negative bearing capacity. The final effect on the hysteresis curve is equivalent to shifting the hysteresis curve downward as a whole, but the specimen still exhibits a full hysteresis curve and a strong energy dissipation capacity. Therefore, when
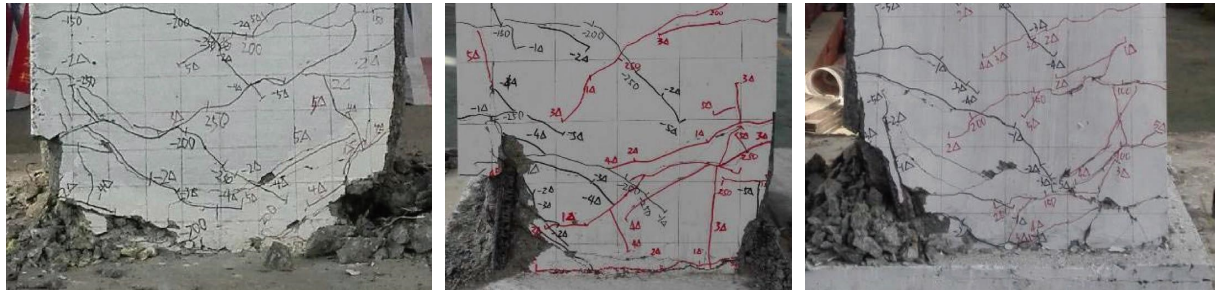
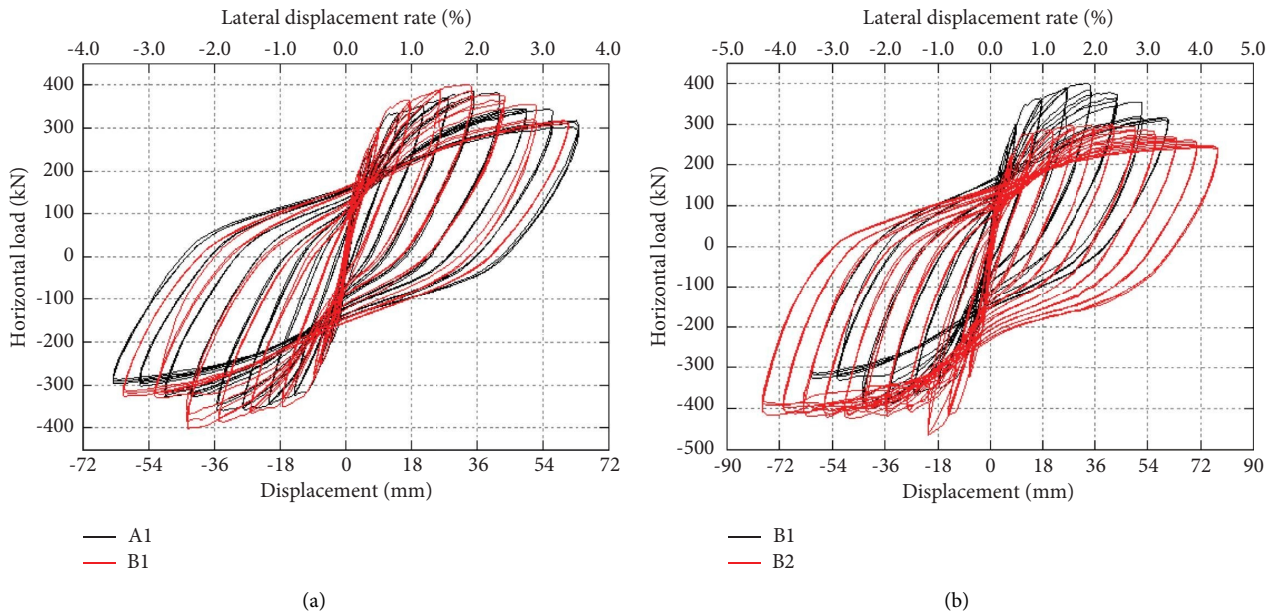FIGURE 6: Plastic hinge failure of each specimen.

(a)

(b)

FIGURE 7: Hysteresis curve of each specimen. (a) Specimens A1 and B1. (b) Specimens B1 and B2.

the bridge is a continuous beam bridge, it is suggested to design the pier so that it has only a small eccentric compression under the action of a dead load, and the simply supported beam pier should meet the axial compression requirement by adjusting the position of the bearing as much as possible. At the same time, it can consider increasing the width of the bent cap to prevent the possible increased risk of falling the beam when the prefabricated pier is subjected to eccentric compression. In addition, for bridges under the same boundary conditions, the pier column section and reinforcement at the node connection should be increased for the prefabricated pier under an eccentric load compared with the prefabricated pier under axial compression, and asymmetric reinforcement can be considered for reinforcement.

4.2. Skeleton Curve. The skeleton curve in Figure 8 shows that the initial stiffness of specimens A1 and B1 was close and that the failure processes of the specimens were similar. In the elastic-plastic stage, with the increasing load-displacement level and cycle number, the slope of the curve decreases and the horizontal load gradually reaches
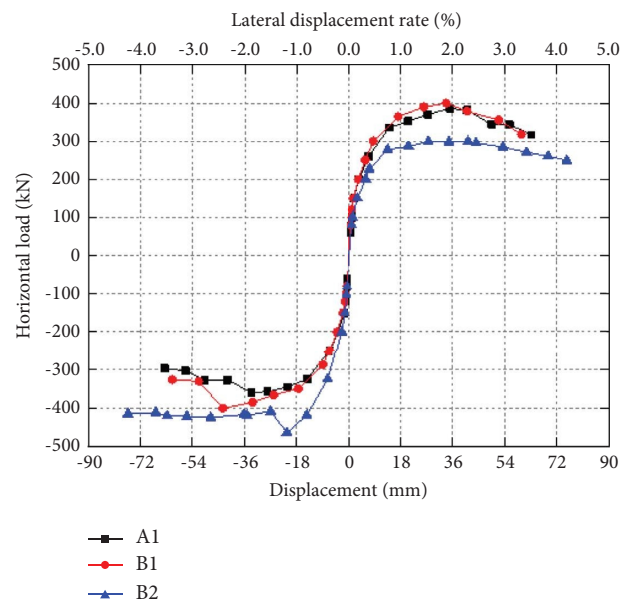

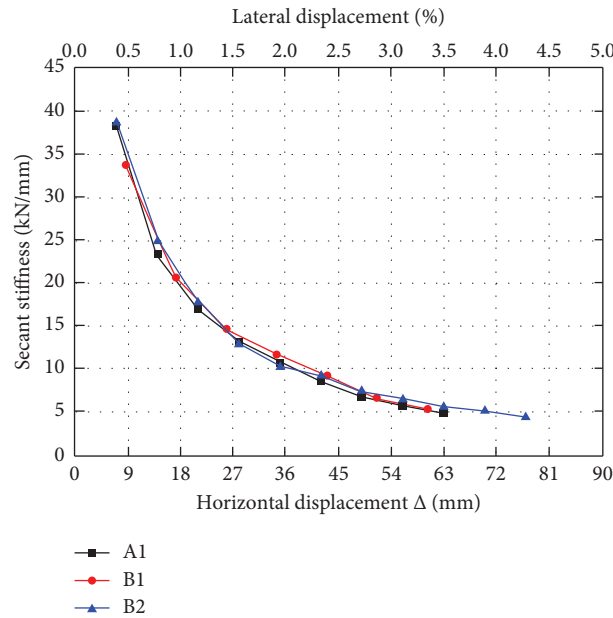FIGURE 8: Skeleton curve of each specimen.

FIGURE 9: Stiffness degradation curve of each specimen.

the peak load of the specimen. After the peak load is reached, the horizontal loads on the specimens in groups A and B begin to decrease gradually, and the specimens begin to enter the failure stage. Finally, a large area of concrete at the bottom of the pier is crushed and peeled off, and the horizontal load decreases to less than 85% of the peak load, reaching the specimen failure standard.

The skeleton curve of specimen B2 shows that the eccentric load can decrease the positive stiffness and increase the negative stiffness, which correlates to the loading position of the eccentric load. Under the eccentric load, the positive horizontal load drops for specimen B2, that is, the strength degradation, is more gradual.

4.3. Stiffness Degradation.
In this article, the equivalent stiffness K_i (secant stiffness) [23] is used to analyze the stiffness degradation of the specimens. As shown in Figure 9, the equivalent stiffness results and variations of the cast-in-place specimen A1 and specimen B1 are very close and basically coincide, indicating that connection with UHPC-grouted corrugated pipes can achieve the same effect as the cast-in-place structure. A comparison between the equivalent stiffness curves of specimens B2 and B1 shows that the equivalent stiffness curve of the specimen under eccentric compression basically coincides with that under axial compression and that the eccentric load has a little effect on the stiffness and stiffness degradation of the specimen.

4.4. Displacement Ductility.
In this article, the yield points of the structure are determined by the geometric drawing method in reference [24], and the ductility factor of each specimen is shown in Table 3.

The table shows that the ductility factor of specimen B1 connected with UHPC-grouted corrugated pipes under axial

compression is slightly smaller than that of CIP specimen A1, approximately 11% smaller in the positive direction and approximately 25% smaller in the negative direction. For the connection of specimen B2 with the UHPC-grouted corrugated pipe under small eccentric compression, the positive ductility factor is 20% higher than that of the CIP specimen A1, and the negative ductility factor is 18.6% higher than that of the cast-in-place specimen A1. The ultimate load of A1 specimen is about 10% less than that of B1 specimen, while the positive ultimate load of B2 specimen decreases significantly, about 22% less than that of A1 specimen, and the negative ultimate load increases significantly, about 29% more than that of A1 specimen.

4.5. Cumulative Energy Dissipation Analysis.
The energy dissipation capacity of the structure is usually evaluated with the cumulative energy dissipation index [25]. Figure 10 shows that when the ultimate displacement grade of test piece B1 is 55 mm, the hysteretic energy consumption of A1 is 3 kN·m less than that of B1, and the cumulative energy consumption of A1 is 33 kN·m greater than that of B1. The difference of the energy consumption capacity between B1 and A1 is not more than 10%, indicating that the connection with the UHPC-grouted corrugated pipes can achieve the same energy dissipation capacity as the CIP structure, that is, they have equivalent seismic performance.

For specimen B2, the eccentric load can enhance the energy dissipation of the specimen, and the energy dissipation capacity of the specimen under eccentric compression is greater than that under axial compression at the same displacement load level. High eccentric load energy dissipation capacity, in consideration of a combined strengthening effect on the pier column from the eccentric load and UHPC, improves the bonding effect of the stressed steel bar and concrete, enlarges the bearing capacity at the same

TABLE 3: Ductility factor of each specimen.

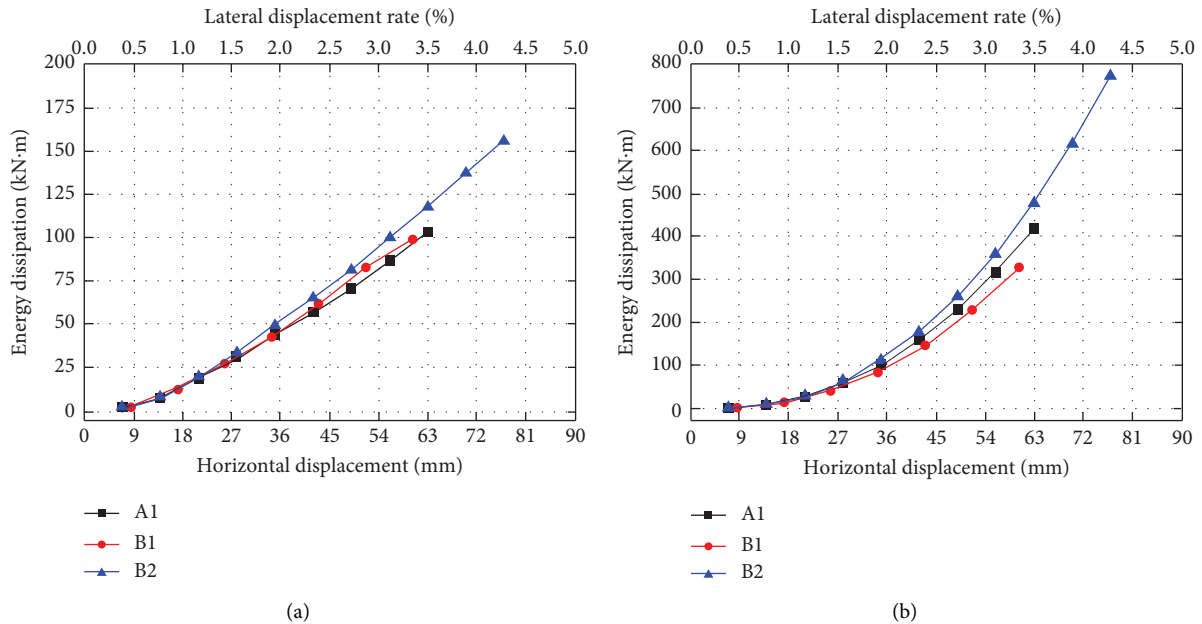| Specimens	Loading directions	Yield displacement (mm)	Yield load (kN)	Peak load (kN)	Ultimate load (kN)	Ultimate displacement (mm)	Ductility factor (μ)
A1	Positive	7.08	260.3	385.4	327.6	60.22	8.5
	Negative	6.41	243.8	−359	−305.2	55.65	8.68
B1	Positive	7.36	278.4	400	340	55.2	7.5
	Negative	8.16	282.5	−400.8	−340.7	50.56	6.2
B2	Positive	7.09	223.3	299	254.1	72.73	10.26
	Negative	7.4	326.9	−465.1	−395.3	76.22	10.3

FIGURE 10: Energy dissipation capacity of each specimen. (a) Energy dissipation of each displacement level. (b) Cumulative hysteretic energy dissipation.

displacement level, and increases the energy dissipation capacity of the pier column. For specimen B2, connected with UHPC-grouted corrugated pipes under small eccentric compression, the hysteretic energy is 20 kN·m greater than that of specimen B1, and the cumulative energy consumption is 48 kN·m greater than the A1 test piece, and the energy consumption capacity is about 10% greater when the displacement load level is 63 mm, also considering the different yield displacements applied in the test. The connection structure of an eccentrically prefabricated pier can be adjusted by comprehensively considering the seismic fortification intensity of the area where the bridge is located. In the low-intensity area, the eccentric compression pier can be considered to be designed in the same way as the axial compression pier to pursue economy. In the high-intensity area, the section and reinforcement of the joint connection should be increased to meet the ultimate bearing capacity and greatly enhance its energy dissipation capacity.

5. Conclusions

In this article, three scaled pier specimens with different connections were tested to study the damage mechanism and their seismic performance. Prefabricated piers using UHPC-grouted corrugated pipe connecting technology under eccentric compression were considered and compared with the CIP specimens. The energy dissipation capacity, ductility performance, and equivalent stiffness were analyzed and compared, and the main conclusions are as follows:

(1) The cracks distribution of specimen B1 which was connected by the UHPC-grouted corrugated pipe was similar to that of specimen A1 using the CIP connection. Specimen B1 had a higher side crack, which indicated that the force can be transferred

effectively by using the UHPC-grouted corrugated pipe connection. The influence of small eccentric compression was to cause longer cracks and more serious concrete crushing damage on the eccentric side significantly.

(2) Compared to the conventional CIP pier, the overall energy dissipation capacity and the ductility factor of the assembled pier with the UHPC-grouted corrugated pipe connection were decreased approximately by 5.0% and by 10%, respectively. The pinching phenomenon of the hysteresis curve of the precast pier was more obvious.

(3) When the assembled piers were under small eccentric compression, the overall energy dissipation capacity was close to that of conventional CIP piers and the ductility factor was improved by 20%. Comparison of two precast piers using the same UHPC grout connections shows that the stiffness degradation process of precast pier under small eccentric compression was similar to that under axial compression. But the ductility coefficient of precast pier under small eccentric compression increased by about 20%.

(4) The small eccentric compression caused different damage degrees in the plastic hinge zone at the bottom of the precast column. It is suggested that the diameter and spacing of stirrups at the joints of precast assembled piers can be properly strengthened, especially under small eccentric compression.

Data Availability

The datasets generated or analyzed during this study are available from the corresponding author on reasonable request.

Conflicts of Interest

The authors declare that they have no conflicts of interest.

Acknowledgments

References

[1] A. Mehrsoroush, M. S. Saiidi, and K. Ryan, *Development of Earthquake-Resistant Precast Pier Systems for Accelerated Bridge Construction in Nevada*, Nevada Department of Transportation, Nevada, 2017.

[2] M. P. Culmo, *Connection Details for Prefabricated Bridge Elements and Systems*, Federal Highway Administration, Washington, D.C, 2009.

[3] C. Fang, D. Liang, Y. Zheng, M. C. Yam, R. Sun, and R. Sun, "Rocking bridge piers equipped with shape memory alloy (SMA) washer springs," *Engineering Structures*, vol. 214, Article ID 110651, 2020.

[4] Y. Zheng, C. Fang, D. Liang, and R. Sun, "An innovative seismic-resilient bridge with shape memory alloy-washer-based footing rocking RC piers," *Journal of Intelligent Material Systems and Structures*, vol. 32, no. 5, pp. 549–567, 2021.

[5] C. S. Shim, Y. S. Chung, and J. Y. Yoon, "Cyclic behavior of prefabricated circular composite columns with low steel ratio," *Engineering Structures*, vol. 33, no. 9, pp. 2525–2534, 2011.

[6] G. Guerrini, J. I. Restrepo, M. Massari, and A. Vervelidis, "Seismic behavior of posttensioned self-centering precast concrete dual-shell steel columns," *Journal of Structural Engineering*, vol. 141, no. 4, Article ID 04014115, 2015.

[7] J. T. Hewes and M. J. N. Priestley, "Seismic design and performance of precast concrete segmental bridge columns," *Rep. No. SSRO-2001/25*, Dept. of Structural Engineering, Univ. of California at San Diego, La Jolla, CA, 2002.

[8] B. Wang, S. Zhu, C. X. Qiu, and H. Jin, "High-performanceself-centering steel columns with shape memory alloy bolts: design procedure and experimental evaluation," *Engineering Structures*, vol. 182, pp. 446–458, 2019.

[9] F. Brenes, S. Wood, and M. Kreger, *Anchorage Requirements for Grouted Vertical-Duct Connectors in Precast Bent Cap Systems 6. Performing Organization Code*, Bridge Anchorages, Anchorage, AK, USA, 2006.

[10] A. G. Wilson, *Emulative Precast Bent Cap Connections for Seismic Regions: Component Tests - Preliminary Grouted Duct Specimen (Unit 5)*, California State University, Sacramento, CA, 2010.

[11] L. S. Bao, Y. B. Zhang, Z. W. Sang, and L. Yu, "Quasi-static test and numerical simulation analysis for seismic performance of fabricated assemble bridge piers base on bellows connection," *China Journal of Highway and Transport*, vol. 31, pp. 242–249, 2018.

[12] J. F. Jia, Y. Guo, N. H. Song, Y. H. Zhu, X. L. Du, and L. Geng, "Seismic testing of precast RC bridge pier columns anchored by grouted corrugated ducts," *China Journal of Highway and Transport*, vol. 31, pp. 211–220, 2018.

[13] E. Fehling, P. Lorenz, and T. Leutbecher, "Experimental investigations on anchorage of rebars in UHPC," in *Proceedings of the Hipermat 2012 3rd International Symposium on UHPC and Nanotechnology for High Performance Construction Materials*, pp. 533–540, Kassel University Press, Kassel, Germany, March 2012.

[14] S. Ichikawa, H. Matsuzaki, A. Moustafa, M. A. ElGawady, and K. Kawashima, "Seismic-resistant bridge columns with ultrahigh-performance concrete segments," *Journal of Bridge Engineering*, vol. 21, no. 9, Article ID 04016049, 2016.

[15] B. A. Graybeal, *Behavior of Ultra-high Performance Concrete Connections between Precast Bridge Deck Elements*, Smart and Sustainable Bridges, Phoenix, AZ, 2010.

[16] J. Chen, Y. Xiao, and Q. Yin, "Bonding strength of rebar anchorage in embedded corrugated sleeve with high strength grout," *Journal of Building Structures*, vol. 36, pp. 140–147, 2015.

[17] F. Qiu, Z. Xia, S. Zhu et al., "Seismic performance analysis of prestressing prefabricated bridge piers with grouting bellows," *Earthq. Eng. Eng. Dyn.* vol. 38, pp. 144–153, 2018.

[18] M. Tazarv and M. S. Saiidi, "UHPC-filled duct connections for accelerated bridge construction of RC columns in high seismic zones," *Engineering Structures*, vol. 99, pp. 413–422, 2015.

[19] J. B. K. Pang, M. O. Eberhard, and J. F. Stanton, "Large-bar connection for precast bridge bents in seismic regions," *Journal of Bridge Engineering*, vol. 15, no. 3, pp. 231–239, 2010.

[20] M. Elsayed and M. L. Nehdi, "Experimental and analytical study on grouted duct connections in precast concrete construction," *Materials and Structures*, vol. 50, no. 4, p. 198, 2017.

[21] H. Jiang, Z. Wang, and J. Shen, "Anti-seismic performance testing of prefabricate asembly pillars connected with grouting metal corrugated pipe," *Structural Engineer*, vol. 32, pp. 132–138, 2016.

[22] Z. Wang, Z. Wei, H. Wei, and W. A. Hao, "Influences of precast segmental connector forms on seismic performance of bridge pier," *China Journal of Highway and Transport*, vol. 30, pp. 74–80, 2017.

[23] Y. Huang, *Study on Seismic Performance of Precast Reinforced Concrete Bridge Piers*, Dalian University of Technology, Dalian, 2016.

[24] H. Jiang, H. Zhang, W. Liu, and H. Y. Yan, "Experimental study on plug-in filling hole for steel bar anchorage of the PC structure," *Journal of Harbin Institute of Technology*, vol. 43, pp. 28–31, 2011.

[25] P. Feng, H. Qiang, and L. Ye, "Discussion and definition on yield points of materials, members and structures," *Engineering Mechanics*, vol. 34, pp. 36–46, 2017.